Available online at www.sciencedirect.com

ScienceDirect

Geochimica et Cosmochimica Acta 241 (2018) 1–16

Geochimica et Cosmochimica Acta

www.elsevier.com/locate/gca

Gibbs Energy Dynamic Yield Method (GEDYM): Predicting microbial growth yields under energy-limiting conditions

Christina M. Smeaton *, Philippe Van Cappellen

Ecohydrology Research Group, Department of Earth and Environmental Sciences and The Water Institute, University of Waterloo, Waterloo, ON N2L 3G1, Canada

Received 11 December 2017; accepted in revised form 10 August 2018; available online 29 August 2018

Abstract

Biomass-explicit biogeochemical models assign microbial growth yields (Y) using values measured in the laboratory or predicted using thermodynamics-based methods. However, Y values are rarely measured under the low energy delivery conditions that often prevail in the subsurface, and existing predictive methods for calculating Y values when the catabolic energy supply rate is limited remain poorly tested. Here, we derive and validate a new semi-theoretical method for calculating Y values: the Gibbs Energy Dynamic Yield Method (GEDYM). Method validation relies on a compilation of 132 geochemically relevant literature Y values comprising predominantly (60%) low energy (> -25 kJ (mol e^-)$^{-1}$) metabolisms. GEDYM is based on estimating the Gibbs energy change of the metabolic reaction (ΔG_{met}), which links the Gibbs energy changes of the catabolic (ΔG_{cat}) and anabolic (ΔG_{an}) reactions of a microorganism through its growth yield. Given that the values of $\Delta G_{met}, \Delta G_{cat}$ and ΔG_{an} all depend on their respective reaction quotients, the resulting Y values account for changes in the chemical environment surrounding the cells. GEDYM incorporates an empirical relationship that accurately estimates the extent to which ΔG_{met} deviates from its standard state value from the relative difference between ΔG_{cat} and its corresponding standard state value. GEDYM yields Y values with lower relative errors and statistical bias than the existing Gibbs energy dissipation method (GEDM). Using dissimilatory iron reduction, sulfate reduction and methanogenesis as examples, we illustrate the importance of considering variations in ΔG_{cat} and ΔG_{an} when predicting Y values for individual metabolisms. Because of its ability to dynamically adjust the values of ΔG_{met} and Y to variable geochemical conditions, GEDYM yields a more realistic representation of geomicrobial activity in predictive reactive transport models.

1. INTRODUCTION

Microorganisms sustain numerous ecosystem functions including, but not limited to, geochemical cycling, bioremediation and ore formation. An understanding of the kinetic and thermodynamic controls on microbial activity is thus paramount to assess and predict the biogeochemical functioning of many natural ecosystems. Kinetic models of microbially mediated reactions are either biomass-implicit or biomass-explicit. The former models assume a steady state biomass distribution and fold the biomass into an empirical, site specific rate constant (e.g., Hunter et al.,1998; van Breukelen et al., 2004; Arora et al., 2016), while the latter explicitly account for microbial growth using growth yields and biomass concentrations (e.g., Istok et al., 2010, Rodríguez-Escales et al., 2016). The standard theoretical basis for simulating microbial growth rates is the Monod model (Monod, 1949) (see Section 2).

* Corresponding author.
E-mail address: christina.smeaton@uwaterloo.ca (C.M. Smeaton).

https://doi.org/10.1016/j.gca.2018.08.023
0016-7037/

The growth yield, conventionally represented by the symbol Y, forms the stoichiometric link between anabolism to catabolism in bioenergetics models. It is defined as the portion of the growth-limiting substrate consumed that is converted into cellular biomass (Lipson, 2015); it is expressed in, for instance, grams of cells per mol of electron donor (e.g., Strohm et al., 2007) or C-mol biomass per C-mol electron donor (e.g. Rutgers et al., 1989). The latter units are particularly useful when comparing different microorganisms growing on the same carbon-based electron donor: Y can then directly be interpreted as a measure of the C-based electron donor use efficiency. For example, a Y value of 0.1 C-mol biomass (C-mol acetate)$^{-1}$ during the oxidation of acetate coupled to the reduction of sulfate implies that 10% of the carbon from acetate is incorporated into new cellular biomass. Many Y values found in the literature are specific for a particular microorganism and metabolism (e.g., Strohm et al., 2007).

Biomass-explicit models that are used to predict substrate utilization rates (e.g., sulfate reduction) range from those describing microbial reaction kinetics in pure cultures (e.g., Liu et al., 2001a) to environmental reactive transport models (RTMs) applied to water bodies (e.g., Reed et al., 2014), groundwaters (e.g., Yabusaki et al., 2007; Li et al., 2009; Bao et al., 2014), lake sediments (e.g., Jin et al., 2013), marine sediments (e.g., Dale et al., 2006), and soils (e.g., Neill and Gignoux, 2006). Given the difficulty of measuring in situ microbial growth yields, a common practice in RTMs is to extrapolate Y values measured in laboratory incubations to field conditions (e.g., Scheibe et al., 2006; Bao et al., 2014). However, in the laboratory, Y values are usually obtained under highly favorable conditions, including optimal temperatures, nutrient-rich growth media and high electron donor and acceptor concentrations (often in the mM range). Depending on the experimental method, Y values are either derived from data collected during exponential growth (i.e., in chemostats), or after the microorganisms have entered the stationary growth phase (i.e., in batch experiments). Therefore, the corresponding Y values reflect growth of a uniform population of cells which have either undergone (i.e., batch) or continue (i.e, chemostats) to experience an energy-replete physiological state characterized by high metabolic rates and rapid growth (e.g., Laanbroek et al., 1984; Strohm et al., 2007). It is thus questionable whether these values apply to microbial populations inhabiting resource-limited environments.

In principle, a detailed knowledge of the complete network of metabolic pathways informed by genomics should allow one to predict the effects of nutrient and electron donor and acceptor supply rates on the growth and function of a given microorganism without the need to assign a growth yield (Mahadevan et al., 2011, and references therein). So-called genome-scale models have successfully been implemented in RTMs (Scheibe et al., 2009). The comparison of a uranium bioremediation RTM, including either a traditional Monod growth model with a specified Y-value or a genome scale metabolic model of *Geobacter sulfurreducens*, yielded higher cell concentrations for the Monod model (Scheibe et al., 2009). The observation was attributed to the constant Y value used in the Monod model, while in the genome-scale model growth dynamically adjusts to the environmental chemical gradients. Not surprisingly, a subsequent sensitivity analysis of a RTM using the traditional Monod model applied to the same aquifer identified Y as a key parameter required to predict the fate of uranium (Zhao et al., 2011). However, for many environments of interest the entire microbial genome is not, or only incompletely, known.

Under energy-limiting conditions, Y can be related to the catabolic energy yield via empirical relationships (e.g., Roden and Jin, 2011) or through bioenergetically based models (Heijnen et al., 1992; McCarty, 2007), such as the Gibbs Energy Dissipation model (GEDM). Models grounded in thermodynamics provide a theoretically sound approach to predict Y values in energy-stressed environments (e.g., subsurface environments). These values can then be implemented into comprehensive microbial kinetic formulations describing substrate consumption or production. Moreover, the experimental determination of Y values when solid phase electron acceptors (or reaction products) are involved may be difficult, for example during dissimilatory reduction of insoluble iron(III) oxyhydroxides, because solids interfere with commonly used optical methods to measure biomass. In these cases, predictive bioenergetic models offer an alternative way to estimate metabolism-specific Y values. Most existing bioenergetic models, however, have been calibrated with data from bioengineering and biotechnological applications that may not provide realistic analogues for the low energy-yielding metabolisms prevailing in many subsurface environments.

VanBriesen (2002) assessed different bioenergetics models by comparing predicted Y values for aerobic respiration to 10 Y values determined in the laboratory. More recently, Kleerebezem and Van Loosdrecht (2010) evaluated the accuracy of the same models using 31 measured Y values for O_2 respiration (74% of the data), denitrification (16%) and methanogenesis (10%). While both reviews show similar errors across the different models (12–20%), they both compared the model predictions to a small number of experimental Y values with a bias towards higher-energy yielding metabolisms. Moreover, the catabolic Gibbs energy values used in the Y prediction models by VanBriesen (2002) and Kleerebezem and Van Loosdrecht (2010) were calculated under biochemical standard state conditions (i.e., 25 °C, pH 7 and unit activities for all chemical species, except H^+), that is, conditions that may deviate significantly from those encountered in environmental systems (LaRowe and Amend, 2015). Thus, for geochemical applications, a Y prediction method should account for the spatial and temporal variable temperature and chemical conditions under which the metabolic processes are occurring.

A key objective of our study is to extend the original Gibbs Energy Dissipation model (GEDM) of Heijnen et al. (1992) and develop a method for calculating Y values that can be implemented in dynamic, biomass-explicit

biogeochemical models. We achieve this by (1) establishing an empirical relationship between the Gibbs energies of catabolism and metabolism using a database comprising 132 experimental Y values, with 60% of values corresponding to low energy yielding catabolic processes (i.e. > -25 kJ/mol e^-), hence including common geomicrobial metabolisms such as methanogenesis and sulfate reduction, and (2) deriving a new Y prediction model from the aforementioned empirical relationship and the original GEDM. While the Y data assembled pertain to catabolic energy production during chemoorganotrophy, chemolithotrophy, methanogenesis, and fermentation, the theoretical framework should provide the foundation to predict Y for other important geomicrobial metabolic classes.

2. BIOGEOCHEMICAL SIGNIFICANCE OF THE GROWTH YIELD

Growth yields are generally incorporated into biomass-explicit microbial kinetic models using the well-known Monod formulation (e.g., Thullner et al., 2007). The biomass production rate (r_x) [in units of biomass (time)$^{-1}$] is a function of the microorganism's specific growth rate (μ) [time^{-1}]:

$$r_x = \mu X \tag{1}$$

where X is the biomass. Note that although μ is referred to as a rate, it is actually a rate coefficient. The value of μ reflects both the microorganism's intrinsic metabolic capacity and the external environmental conditions. The Monod microbial growth equation (Monod, 1949) relates μ to the availability of a growth-limiting substrate via:

$$\mu = \mu_{max}\frac{S}{K_s + S} \tag{2}$$

where μ_{max} is the maximum specific growth rate [time^{-1}], S is the concentration of the substrate, and K_s is the substrate affinity constant, that is, the substrate concentration when $\mu = 0.5\mu_{max}$.

The growth yield (Y) directly couples the rate of substrate consumption (r_s) [mass substrate (time^{-1})] to the biomass production rate:

$$r_s = \frac{1}{Y}r_x \tag{3}$$

(Note that the additional substrate consumption required to enable the cellular maintenance processes can be accounted for by adding an extra term to the RHS of Eq. (3), commonly known as the maintenance substrate utilization rate, m_s [moles substrate (C-mol biomass h)$^{-1}$].) Combining Eqs. (1), (2) and (3):

$$r_s = -\frac{\mu_{max}}{Y}\cdot X \cdot \frac{S}{K_s + S} \tag{4}$$

The Monod formulation can be expanded to multiple substrates. For example, for energy-limited growth, where the catabolic reaction involves the transfer of electrons from an external electron donor (S_d) to a terminal electron acceptor (S_a), a multiplicative formulation can be used:

$$r_s = -\frac{\mu_{max}}{Y}\cdot X \cdot \left(\frac{S_a}{K_a + S_a}\right)\cdot\left(\frac{S_d}{K_d + S_d}\right) \tag{5}$$

A key thermodynamic condition that applies to cellular metabolism is that the catabolic reaction must be generating useable energy under the prevailing environmental conditions, that is, $\Delta G_{cat} < 0$, where ΔG_{cat} [kJ mol^{-1}] is the Gibbs energy change of the catabolic reaction under non-standard conditions:

$$\Delta G_{cat} = \Delta G^{\circ}_{cat} + RTlnQ_{cat} \tag{6}$$

where ΔG°_{cat} is the Gibbs energy of the catabolic reaction under standard conditions and Q_{cat} is the corresponding reaction quotient. In addition, it has been observed that a minimum excess catabolic energy production is required for cells to be able to utilize a given catabolic reaction. This requirement can be explicitly added to the Monod model. Jin and Bethke (2003, 2007), for instance, propose the following formulation:

$$r_s = -\frac{\mu_{max}}{Y}\cdot X \cdot \left(\frac{S}{K_s + S}\right)\cdot\left(1 - exp\left(\frac{\Delta G_{cat} + n\Delta G_{ATP}}{\chi RT}\right)\right) \tag{7}$$

where the corresponding thermodynamic condition now states that the catabolic reaction will proceed at the rate given by Eq. (7) when $(\Delta G_{cat} + n\Delta G_{ATP}) < 0$; when $(\Delta G_{cat} + n\Delta G_{ATP}) > 0$, the reaction can no longer sustain the metabolic machinery of the cells, and $r_s = 0$. In Eq. (7), ΔG_{ATP} [kJ mol^{-1}] is the Gibbs energy required to produce 1 mol of ATP from ADP and monophosphate, n is the number of ATP molecules produced per catabolic formula reaction, R is the universal gas constant, T is the absolute temperature, and χ is the average stoichiometric number. The latter is the number of times the rate limiting step occurs per overall reaction and is often related to proton translocation across the cell membrane (Jin and Bethke, 2003). An alternative formulation for the last term on the right hand side (RHS) of Eq. (7) has been proposed by LaRowe et al. (2012), based on the minimum energy requirement to sustain a viable cell membrane potential.

The use of an energy explicit equation such as Eq. (7) rather than Eq. (4) is crucial under energy-limiting conditions, that is, when the absolute value of ΔG_{cat} approaches $n\Delta G_{ATP}$. In that case, most energy generated by catabolism is diverted to maintenance functions, with little energy left to invest in growth. Thus, it may seem that with the last term on the RHS of Eq. (7), the dependence of microbial reaction kinetics on energy limitation is accounted for. However, the value of Y is also dependent on catabolic energy gains (Roden and Jin, 2011). In what follows, we focus specifically on how to relate Y to the energetics of cellular metabolism.

3. EXPERIMENTAL DATA: LITERATURE COMPILATION

Experimental growth yields and ancillary data are based on an extensive literature search predicated on electron-donor (ED) limited monoculture growth on C1-C6 carbon

sources and H_2: in total, 132 growth yields are used (for a complete listing including the anabolic and catabolic reactions, see Tables A.1 and B.1). In what follows and unless otherwise denoted, the Y values are expressed in units of C-mol biomass per C-mol ED, except when H_2 is the electron donor and Y is expressed as C-mol biomass per mol H_2. The data set includes 96 Y values selected from the 123 values assembled by Roden and Jin (2011); 30 values are excluded because of the lack of chemical data to calculate Gibbs energies of reaction under non-standard state conditions, or because the values correspond to syntrophic growth. Ancillary data include pH, temperature, aqueous chemical concentrations and the experimental method (i.e., batch, chemostat or retentostat).

The anabolic reactions are all written using the generic microbial biomass formula of $C_5H_9O_{2.5}N$ (or $CH_{1.8}O_{0.5}N_{0.2}$), proposed by Roels (1980) based on the measured elemental concentrations of eight microbial species. This biomass formula gives a corresponding molecular weight of 24.6 g (C-mol biomass)$^{-1}$. The anabolic reactions account for the differences in C oxidation states between the carbon source and the biomass (Kleerebezem and Van Loosdrecht, 2010). Details on how the anabolic formula reactions are derived are provided in Section 3 and Appendix C.1. Standard state Gibbs energy changes of the anabolic (ΔG°_{an}), catabolic (ΔG°_{cat}) and metabolic (ΔG°_{met}) reactions are calculated using the standard Gibbs energies of formation (ΔG°_f) of the products and reactants at 298.15 K.

Gibbs energies and enthalpies of formation (ΔG°_f and ΔH°_f) of the relevant chemical species are obtained from Shock (1995), Stumm and Morgan (1996), Shock et al. (1997) and Majzlan et al. (2004). ΔG°_f values are unavailable for iron citrate complexes, therefore formation constants (i.e., log$K$ values) from Wang et al. (2008) are converted to ΔG°_f, giving values of −2450.4 and −2460.08 kJ/mol for $Fe(C_6H_5O_7)_2^{3-}$ and $Fe(C_6H_5O_7)_2^{4-}$, respectively. Likewise, log$K$ values from Dong and Brooks (2006) are used to calculate the ΔG°_f of $MgUO_2(CO_3)_3^{2-}$, $Ca_2UO_2(CO_3)_4$ and $CaUO_2(CO_3)_3^{2-}$ complexes, giving values of −3140.1, −3817.1 and −3231.8 kJ/mol, respectively. The remaining ΔG°_f for the relevant uranium complexes and uraninite are those of Guillaumont et al. (2003). For biomass, we rely on the ΔG°_f and ΔH°_f values of Roels (1980), −67 and −91.4 kJ (C-mol biomass)$^{-1}$, respectively. These values, which are the only ones currently available in the literature, have previously been successfully implemented in other bioenergetic models (e.g., Heijnen and Van Dijken, 1992).

Standard Gibbs energies of reaction are corrected for experimental temperatures using the Gibbs-Helmholtz equation:

$$\Delta G^\circ_{rT} = \Delta G^\circ_{r298} \cdot \left(\frac{T}{298.15}\right) + \Delta H^\circ_{r298} \cdot \left(\frac{298.15 - T}{298.15}\right) \quad (8)$$

where ΔH°_{298} is the standard enthalpy change at 298.15 K, and T is the experimental temperature in Kelvin. Gibbs energies of reaction under non-standard state conditions are calculated according to:

$$\Delta G_r = \Delta G^\circ_{rT} + RTlnQ \quad (9)$$

where ΔG°_r is the Gibbs energy of reaction under standard state conditions corrected for temperature using Eq. (8) and Q is the reaction quotient. Chemical concentrations are converted to activities using PHREEQC v.3 (Parkhurst and Appelo, 2013). Chemical concentrations are those either directly measured when the final biomass was collected, or computed from the initial concentrations by applying appropriate formula reactions to calculate the final concentrations when the biomass was collected. Ionic strengths are estimated from the aqueous and gaseous chemical compositions of the growth medium recipes listed for each literature Y value. Biomass is treated as an insoluble precipitate and assigned an activity of 1 (Battley, 1992).

Specific growth rates (μ) are either taken directly from the experimental studies, or calculated by converting the reported doubling times (t_d) using:

$$\mu = \frac{\ln\ 2}{t_d} \quad (10)$$

When μ or t_d are not reported, the biomass growth curve is digitized with the open source software, Plot Digitizer©, and t_d calculated as:

$$t_d = \frac{0.301(t_2 - t_1)}{\log X_2 - \log X_1} \quad (11)$$

where X_1 and X_2 are cell concentrations measured at times t_1 and t_2 during the exponential growth phase, respectively.

A boxplot of growth yields grouped according to the major electron accepting, methanogenic and fermentation pathways is shown in Fig. 1A. As can be seen, there is a general tendency for Y values to be higher for pathways such as aerobic respiration and denitrification that are associated with the stronger oxidants. However, there is much overlap between the pathways, as any given pathway can exhibit a significant range in Y values. For instance, Y values for chemoorganotrophic aerobic respiration vary between 0.07 and 0.66 C-mol biomass (C-mol ED)$^{-1}$. The majority of doubling times in the experiments included in Fig. 1A fall below 24 h, which reflects the bias in culture studies towards higher specific growth rates (Fig. 1B). Nonetheless, the data set also includes Y values in the slow growth rate regime, which tend to be associated with low energy-yielding processes, such as sulfate reduction and methanogenesis. As also shown by Roden and Jin (2011), a general positive correlation, or linear free energy relationship (LFER), is observed between the measured Y values and the corresponding Gibbs energy changes of the catabolic reaction, ΔG_{cat} (see Appendix Section C.2 and Figs. C1 and C2).

4. ANABOLIC REACTION FORMULAS

The key to predicting Y, and therefore accurately representing geomicrobial processes in biogeochemical models, is

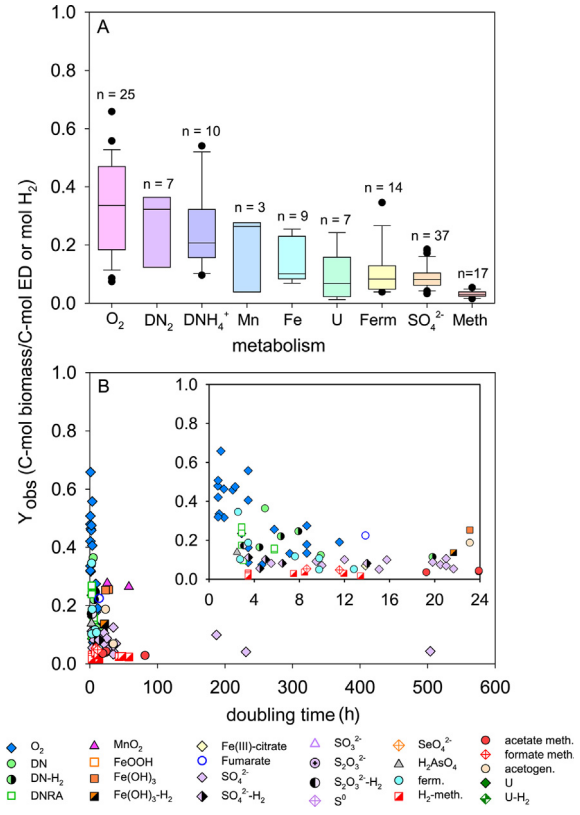

Fig. 1. Compiled literature values of (A) observed Y for the major electron accepting, fermentation (ferm) and methanogenic (meth) metabolic pathways. The black circles represent outliers; DN_2 and DNH_4^+ refer to dissimilatory nitrate reduction to N_2 and NH_4^+, respectively; (B) observed Y plotted versus doubling times where the inset shows data for doubling times less than 24 h; Y is reported as C-mol biomass per mol H_2 for the corresponding catabolic reactions denoted in the legend where H_2 is the electron donor.

to determine the energy demand associated with growth (Kleerebezem and Van Loosdrecht, 2010). The latter is embodied by the anabolic reaction. Consider for example heterotrophic growth with acetate as sole carbon source and electron donor. Production of biomass is then given by:

$$0.5C_2H_3O_2^- + 0.2NH_4^+ + 0.5H^+ + 0.2e^- \rightarrow CH_{1.8}O_{0.5}N_{0.2} + 0.5H_2O \quad (12)$$

where the required electrons are provided by the oxidation of acetate:

$$0.025C_2H_3O_2^- + 0.1H_2O \rightarrow 0.05HCO_3^- + 0.225H^+ + 0.2e^- \quad (13)$$

combining Eqs. (12) and (13) then yields the full anabolic reaction:

$$0.525C_2H_3O_2^- + 0.2NH_4^+ + 0.275H^+ \rightarrow CH_{1.8}O_{0.5}N_{0.2} + 0.05HCO_3^- + 0.4H_2O \quad (14)$$

We define the parameter v as the number of moles of ED used in the synthesis of 1 C-mol of biomass, that is, v corresponds to the stoichiometric coefficient of the ED in the full anabolic formula reaction written to yield 1 C-mol of biomass. In Eq. (14), v equals 0.525 moles of acetate consumed per C-mol of biomass synthesized. When using a different biomass formula, the anabolic formula reaction must be adjusted accordingly (see also Section 7).

In the above example, the carbon source and ED are the same chemical compound, which does not have to be the case. For instance, *Desulfovibrio vulgaris* can grow using sulfate as terminal electron acceptor, H_2 as electron donor and both acetate and carbon dioxide as carbon sources (Badziong et al., 1978). The latter authors report that 70% and 30% of cell carbon derives from acetate and carbon dioxide, respectively. Therefore, the biomass production reaction is given by:

$$0.35C_2H_3O_2^- + 0.3CO_2 + 0.2NH_4^+ + 1.55H^+ + 1.4e^- \rightarrow CH_{1.8}O_{0.5}N_{0.2} + 0.8H_2O \quad (15)$$

The electron donor (H_2) in the catabolic reaction provides the electrons to balance Eq. (15) via:

$$0.7H_{2(aq)} \rightarrow 1.4H^+ + 1.4e^- \quad (16)$$

combining reactions Eqs. (15) and (16) then yields the full anabolic reaction:

$$0.35C_2H_3O_2^- + 0.3CO_2 + 0.2NH_4^+ + 0.7H_{2(aq)} + 0.15H^+ \rightarrow CH_{1.8}O_{0.5}N_{0.2} + 0.8H_2O \quad (17)$$

and v equals 0.7 moles of H_2 per 1 C-mol of biomass synthesized.

The chemolithoautotrophic methanogen, *Methanosarcina barkeri*, is another example of a microorganism where the electron donor and carbon source are different: H_2 is the electron donor and HCO_3^- the carbon source (Smith and Mah, 1978). Biomass production requires the transfer of electrons to bicarbonate according to:

$$HCO_3^- + 0.2NH_4^+ + 5H^+ + 4.2e^- \rightarrow CH_{1.8}O_{0.5}N_{0.2} + 2.5H_2O \quad (18)$$

where the electrons are supplied by:

$$2.1H_{2(aq)} \rightarrow 4.2H^+ + 4.2e^- \quad (19)$$

Combining reactions (18) and (19) yields the full anabolic reaction for *M. barkeri*:

$$HCO_3^- + 2.1H_{2(aq)} + 0.2NH_4^+ + 0.8H^+ \rightarrow CH_{1.8}O_{0.5}N_{0.2} + 2.5H_2O \quad (20)$$

with v equal to 0.1 moles of H_2 used per 1 C-mol of biomass synthesized. Further examples of how to formulate anabolic reactions are given in Appendix C.1.

5. METABOLIC ENERGY BALANCE

If we define λ_{cat} as the number of times the catabolic reaction must proceed in order to meet the energy demand for growth, then the metabolic energy balance is Kleerebezem and Van Loosdrecht (2010):

$$\Delta G_{met} = \lambda_{cat} \cdot \Delta G_{cat} + \Delta G_{an} \quad (21)$$

where ΔG_{met} is in units of kJ (C-mol biomass)$^{-1}$ and corresponds to the Gibbs energy change of the metabolic reaction, that is, the overall reaction coupling catabolic and anabolic reaction (see Section 7 for an example of a metabolic reaction). Note that the metabolic energy balance only accounts for the catabolic energy invested in anabolism. It therefore differs from the total cellular energy balance, which also includes the energy required to perform maintenance processes. In a biomass-explicit microbial kinetic model, the maintenance energy requirement is implemented separately through the substrate utilization rate (see Section 2 and Pirt, 1965, for further details).

The growth yield Y and λ_{cat} are directly related to one another via:

$$\lambda_{cat} = \frac{1 - Yv}{Y} \tag{22}$$

where λ_{cat} is expressed in units of mol ED per C mol biomass, and Y is expressed in C-mol biomass per mol ED. By combining Eqs. (21) and (22) we can express Y in terms of the Gibbs energies of catabolism, anabolism and metabolism (see also Heijnen et al., 1992; Kleerebezem and van Loosdrecht, 2010):

$$Y = \frac{\Delta G_{cat}}{\Delta G_{met} + \Delta G_{cat} v - \Delta G_{an}} \tag{23}$$

where Y is in units of C-mol biomass (mol ED)$^{-1}$. Alternatively, when the ED is an organic compound, Y may be converted to units of C-mol biomass (C-mol electron donor)$^{-1}$ via:

$$Y = \frac{\Delta G_{cat}}{\Delta G_{met} + \Delta G_{cat} v - \Delta G_{an}} \times \frac{1}{\eta_C} \tag{24}$$

where η_C is the number of carbon atoms in the molecular formula of the C-source.

Once the corresponding formula reactions are established, the Gibbs energies of reaction ΔG_{cat}, ΔG_{an} and ΔG_{met} can in principle be calculated at any given temperature and chemical composition of the medium (Section 2). However, to formulate the metabolic reaction from the catabolic and anabolic reactions, λ_{cat} and, therefore, Y must be known. In other words, Eqs. (23) and (24) contain two unknowns, ΔG_{met} and Y. A second equation is therefore required to independently estimate ΔG_{met} in order to use Eqs. (23) or (24) to predict Y. In the next two sections, we describe two methods for obtaining ΔG_{met} values, first the original equation developed by Heijnen and Van Dijken (1992) (Section 5) followed by our new method (Section 6).

6. GIBBS ENERGY DISSIPATION METHOD (GEDM)

The empirical GEDM formula of Heijnen and Van Dijken (1992) is based on 46 growth yields measured for monocultures of aerobes, denitrifiers, chemolithoautotrophs and fermenters supplied with carbon sources containing 1 to 6 C atoms. Because of the general lack of chemical data on the growth media required to calculate reaction quotients, Heijnen and Van Dijken (1992) rely on biochemical standard state Gibbs energies. Fitting of the observed Y values then yields the following empirical formula for the biochemical standard state Gibbs energy of metabolism, $\Delta G^{\circ\prime}_{met}$ [kJ (C-mol biomass)$^{-1}$]:

$$\Delta G^{\circ\prime}_{met} = -\left[200 + 18(6 - \eta_C)^{1.8} + exp\left[\left((3.8 - \gamma_C)^2\right)^{0.16} * (3.6 + 0.4\eta_C)\right]\right] \tag{25}$$

where γ_C is the degree of reduction of C in the carbon source, that is, the number of electrons released per C during complete oxidation to CO_2 (for details on γ_C, see Appendix, section C.1).

According to Eq. (25), $\Delta G^{\circ\prime}_{met}$ depends on the carbon source for anabolism, via η_C and γ_C, but not on the electron acceptor in the catabolic reaction. Energy dissipation (i.e., $-\Delta G^{\circ\prime}_{met}$) is lowest for microorganisms growing on a C source with γ_C values between 3.5 and 4.5. Moreover, for C sources with the same γ_C, energy dissipation is lowest for the C source containing more C atoms. Thus, $-\Delta G^{\circ\prime}_{met}$ decreases the more chemically similar the C source is to intracellular biomass-building compounds, such as pyruvate or acetyl-CoA. Using Eq. (25), $\Delta G^{\circ\prime}_{met}$ values range between −200 and −800 kJ (C-mol biomass)$^{-1}$ for chemoheterotrophs. For chemolithoautotrophs that derive energy using a reverse electron transport (RET) system, Heijnen and Van Dijken (1992) further propose to impose a constant $\Delta G^{\circ\prime}_{met}$ value of −3500 kJ (C-mol biomass)$^{-1}$ and −1000 kJ (C-mol biomass)$^{-1}$ for autotrophs lacking a RET.

For each experimental Y value compiled in our study, the corresponding predicted GEDM Y value is calculated with Eqs. (22) and (23) for H_2 or the carbon based ED, respectively, using the values of ΔG_{cat}, ΔG_{an},v and η_C listed in Appendix Table A1, plus $\Delta G^{\circ\prime}_{met}$ obtained with Eq. (25). The resulting parity plot shows reasonable agreement between the observed and predicted growth yields when considering the entire range of Y values (Fig. 2A). Focusing on the low growth yields (i.e., $Y \leq 0.2$ C-mol biomass (C-mol ED)$^{-1}$), however, reveals significant scatter (inset of Fig. 2A). In addition, the residuals for $Y \leq 0.2$ are not randomly distributed. In particular, the GEDM-calculated Y values of sulfate reduction tend to be systematically lower than the observed values (Fig. 2B).

The $\Delta G^{\circ\prime}_{met}$ values calculated with Eq. (25) can also be directly compared to the experimental ΔG_{met} values in our data set (Fig. 3A). The latter can be derived for each observed Y value by rearranging Eq. (23) and solving:

$$\Delta G_{met} = \frac{-Y\Delta G_{cat} v + Y\Delta G_{an} + \Delta G_{cat}}{Y} \tag{26}$$

The poor agreement in Fig. 3A between experimental and GEDM Gibbs energies of metabolism reflects the inability of Eq. (25) to account for changes in temperature, ED and medium composition. In other words, for a given metabolic pathway, GEDM yields a single value of $\Delta G^{\circ\prime}_{met}$, while in reality ΔG_{met} varies with temperature and changes in the reaction quotient. This limits the usefulness of GEDM in geochemical and environmental applications where large

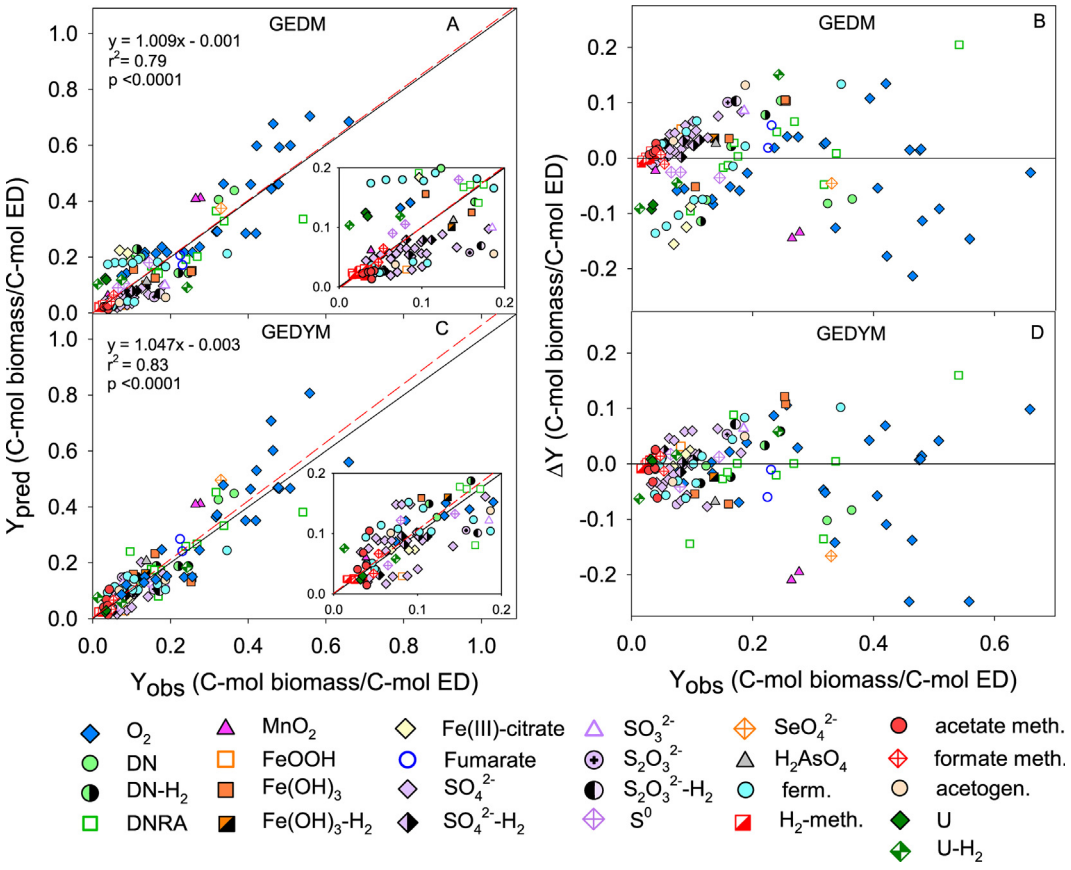

Fig. 2. Parity plots of observed growth yields (Y_{obs}) versus predicted growth yields (Y_{pred}) using (A) GEDM and (C) GEDYM for the major electron accepting and fermentation (ferm) and methanogenic (meth) metabolic pathways. DN and DNRA refer to dissimilatory nitrate reduction to N_2 and NH_4^+, respectively. The inset graphs magnify the x- and y-axis to illustrate model predictions at low growth yields. The black lines represents the 1:1 line while the red dashed lines are the result of linear regression fits. Residual plots of the observed growth yields (Y_{obs}) versus the residuals of the prediction, i.e., ($Y_{obs} - Y_{pred}$) using (B) GEDM, and (D) GEDYM. All Y values are expressed as C-mol biomass/C-mol of electron donor except for those denoted with H_2 in the legend which are expressed as C-mol biomass/mol H_2.

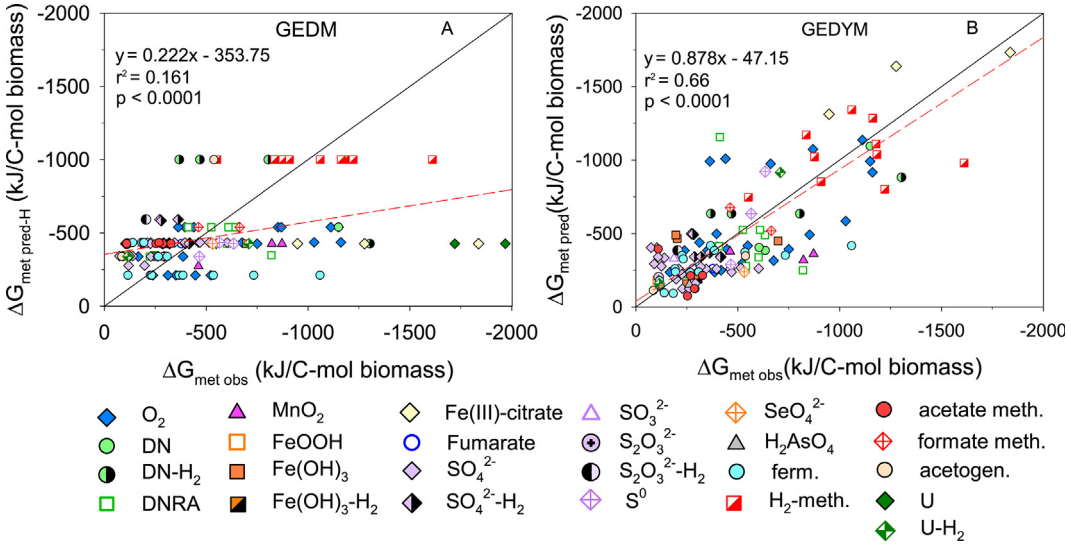

Fig. 3. Parity plots of observed and predicted ΔG_{met} values calculated using (A) the original GEDM, and (B) GEDYM of the major electron accepting and fermentation (ferm) and methanogenic (meth) metabolic pathways. DN and DNRA refer to dissimilatory nitrate reduction to N_2 and NH_4^+, respectively. The black lines represent the 1:1 line while the red dashed lines are the result of linear regression fits.

spatial and temporal gradients in physical, chemical and redox conditions are encountered. Below, we present a novel approach to overcome this limitation of GEDM.

7. GIBBS ENERGY DYNAMIC YIELD METHOD (GEDYM)

The extension of the original GEDM, GEDYM, is based on the highly significant correlation ($r^2 = 0.998$, $p < 0.0001$) observed between the extent to which ΔG_{met} deviates from its standard state value ΔG°_{met} and the corresponding deviation between ΔG_{cat} and ΔG°_{cat} (Fig. 4A):

$$\frac{\Delta G_{met}}{\Delta G^{\circ}_{met}} - 1 = \left(\frac{\Delta G_{cat}}{\Delta G^{\circ}_{cat}} - 1\right) m + b \tag{27}$$

where m and b are the slope and y-intercept, respectively. With Eqs. (23) and (27), we now have a system of two equations for the two unknowns Y and ΔG_{met}. Solving for Y yields:

$$Y = \frac{\alpha \Delta G^{\circ 2}_{cat} - \beta \Delta G^{\circ}_{cat} \Delta G_{cat}}{\alpha v \Delta G^{\circ 2}_{cat} - \Delta G^{\circ}_{cat}\left(\beta v \Delta G_{cat} + \alpha \Delta G^{\circ}_{an} + \Delta G_{an}\right) + m \Delta G_{cat} \Delta G^{\circ}_{an}} \tag{28}$$

where

$$\alpha = m - b - 1 \tag{29}$$

and

$$\beta = m - 1 \tag{30}$$

In Eq. (28), Y is expressed in C-mol biomass (mol ED)$^{-1}$; these units can be converted to C-mol biomass (C-mol ED)$^{-1}$ by dividing the RHS of Eq. (28) by η_C. For growth on mixed electron donors (e.g., H_2 plus $C_2H_3O_2^-$) individual Y values can be determined for each ED. These values can then be converted to common units of C-mol biomass (mol electrons transferred)$^{-1}$, and combined to an overall Y value based on the stoichiometry of the catabolic reaction.

Eq. (27) holds across a remarkably broad range of metabolisms and Y values. Detailed scrutiny of the data reveals that the following metabolisms depart the most from the linear regression in Fig. 4A: (1) aerobic respiration coupled to glucose oxidation (n = 5), (2) glucose fermentation (n = 8), (3) hydrogenotrophic methanogenesis (n = 10), and (4) uranium reduction (n = 5) (Fig. C3). Table 1 therefore provides separate linear fitting parameter values for these four metabolisms. Possible reasons why the four metabolisms deviate from the general trend include uncertainties in the formulation of the catabolic reaction, overflow metabolism and cellular energy sinks other than biomass production.

In the five studies on aerobic glucose oxidation examined (Table A.1, CR# 1-5), secondary oxidation products (i.e., acetate) were only analyzed in one of them (Andersen and von Meyenburg, 1980). Acetate production has been reported to occur at doubling times less than 55 minutes (Basan et al., 2015), which applies to three of the five Y values in our database. For these three Y values we included acetate as a catabolic reaction product (see

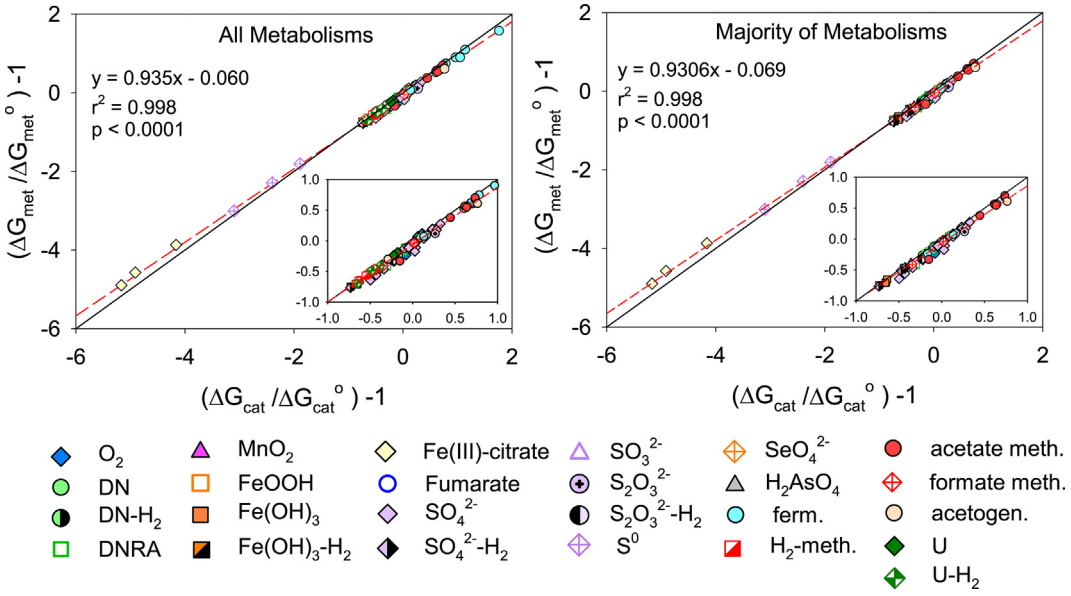

Fig. 4. (A) Parity plots of the ratios of metabolic and catabolic energies under standard versus non-standard conditions (i.e., $\left(\left(\Delta G_{met}/\Delta G^{\circ}_{met}\right) - 1\right)$ versus $\left(\left(\Delta G_{cat}/\Delta G^{\circ}_{cat}\right) - 1\right)$) of (A) all compiled literature growth yields (n = 132), and (B) the majority of metabolisms (n = 102) including all of the major electron accepting, fermentation (ferm) and methanogenic (meth) metabolic pathways. DN and DNRA refer to dissimilatory nitrate reduction to N_2 and NH_4^+, respectively. The inset graphs magnify the x- and y-axis to illustrate the linear relationship for $(\Delta G_{cat}/\Delta G^{\circ}_{cat})$ −1 varying between −1 and +1. The black lines represents the 1:1 prediction line while the red dashed lines are the result of linear regression fits. (For interpretation of the references to colour in this figure legend, the reader is referred to the web version of this article.)

Table 1
The slopes (m) and y-intercepts (b) derived from the empirical relationship between the ratios of metabolic and catabolic energies under standard versus non-standard state conditions presented in Figs. 4B and C3.

Metabolism	m	b	α^{*}	β^{**}
Majority of metabolisms	0.9306	−0.0690	−0.0004	−0.0694
Glucose + oxygen respiration	0.9862	0.0109	−0.0247	−0.0138
Glucose fermentation	0.9048	0.0024	−0.0976	−0.0952
Hydrogenotrophic methanogenesis	0.9975	−0.0225	0.0200	−0.0025
U(VI) reduction	1.0560	0.0029	0.0531	0.0560

* $\alpha = m - b - 1$.
** $\beta = m - 1$.

Table B.1, CR# 2-4). However, there are no actual compositional data to corroborate the catabolic reaction formulas used. Moreover, overflow metabolism has been observed for glucose oxidation in the presence of O_2: bacteria such as *E. coli* may use fermentation rather than respiration as a strategy to lower the energetic demand for proteins synthesis (Basan et al., 2015). For glucose fermenting bacteria, the absence of an external electron acceptor results in greater energy expenditure as compared to non-fermenting microbes. Another potential explanation is that the Y values included in our database correspond to *Clostridium* sp. known to produce endospores that may represent an energy sink not accounted for in our approach. For hydrogenotrophic methanogenesis extra energetic costs may be linked to the use of CO_2 as a carbon source which is highly oxidized and must be reduced to same oxidation state of biomass (i.e, autotrophy) and, for uranium reduction, to those invested in uranium detoxification (Belli et al., 2015).

A parity plot of observed versus Y values calculated with Eq. (28) and the parameter values in Table 1 yields closer agreement of GEDYM with the available data than the original GEDM (Fig. 2), in particular at Y values less than 0.2 C-mol biomass (C-mol ED)$^{-1}$ (see inset on Fig. 2C). The better performance of GEDYM in predicting Y is consistent with the improved estimation of ΔG_{met} using Eq. (28) rather than Eq. (25), as shown by comparing Fig. 3A and 3B. The good performance of Eq. (27) at low Y values likely reflects the corresponding high values of λ_{cat} (see Eq. (14)), which imply that variations of ΔG_{met} are dominated by variations of ΔG_{cat} (see Eq. (13)).

Changes in the biomass formula requires re-writing the anabolic reaction stoichiometry and, therefore, adjusting the values of ΔG°_{an} and ΔG_{an} in Eq. (28). For instance, Liu et al. (2001b) report a biomass formula $CH_{1.64}O_{0.53}N_{0.22}$ for the methanogen *Methanosarcina barkeri*. Use of this biomass formula in Eq. (28) can be compared to that of the generic one for the same microorganism (denoted CR#123 in Tables A.1 and B.1). The predicted Y values with the generic biomass formula ($CH_{1.8}O_{0.5}N_{0.2}$) and the reported biomass formula ($CH_{1.64}O_{0.53}N_{0.22}$) do not vary significantly: they are 0.047 and 0.050 C-mol biomass (C-mol acetate)$^{-1}$, respectively. Both predicted Y values compare equally well to the actual Y measured by Smith and Mah (1978) of 0.039 C-mol biomass (C-mol acetate)$^{-1}$. Nonetheless, more work should be devoted to potential impacts of variable cell biomass composition on growth yield estimations.

8. APPLYING GEDYM: EXAMPLE

As an example of the use of GEDYM, we consider the reduction of amorphous ferric oxide, $Fe(OH)_3$, coupled to the oxidation of acetate by *Geobacter sulfurreducens*, a common subsurface bacterium (Methe et al., 2003), under the controlled laboratory conditions described by Caccavo et al. (1994) (Table A.1, CR# 49). Full details on the experimental conditions and calculations can be found in the Appendix (Table C.1). The anabolic reaction is Eq. (7) and the value of v is 0.525 mol acetate (C-mol biomass)$^{-1}$ (Section 3). The values of ΔG°_{an} and ΔG_{an} are 17.8 and 37.0 kJ (C-mol biomass)$^{-1}$, respectively. The catabolic reaction is:

$$8Fe(OH)_3 + C_2H_3O_2^- + 15H^+ \rightarrow 8Fe^{2+} + 8Fe(OH)_3 + 2HCO_3^- + 20H_2O \quad (31)$$

Note that we use aqueous Fe^{2+} as the reduced reaction product. The latter usually transforms into a ferrous iron solid phase, such as magnetite or siderite. However, the mineral precipitation process is an abiotic reaction from which the bacteria gain no energy. The production of Fe^{2+} in the study of Caccavo and coworkers, as in the case of all the iron reduction studies included in our database, is determined by measuring Fe^{2+} in 0.5 M HCl extracts, which include aqueous as well as solid-bound Fe^{2+}. Therefore, we compute equilibrium aqueous Fe^{2+} activities with respect to the observed secondary iron mineral. In the example here, equilibrium with magnetite yields an Fe^{2+} activity of 2.9×10^{-7}. The corresponding $\Delta G^{\circ}_{cat}$and ΔG_{cat} values are then −475.9 and −173.1 kJ (mol acetate)$^{-1}$.

With the above Gibbs energy changes, Eq. (28) predicts a Y value of 0.159 C-mol biomass (C-mol acetate)$^{-1}$, which compares well to the experimental value of 0.105 C-mol biomass (C-mol acetate)$^{-1}$. From the predicted Y value, we obtain a λ_{cat} value of 2.62 moles acetate (C-mol biomass)$^{-1}$ with Eq. (22). Next, the full metabolic reaction is obtained by adding the anabolic reaction (Eq. (14)) and the catabolic reaction (Eq. (31)) multiplied by λ_{cat}:

$$20.98Fe(OH)_3 + 3.15C_2H_3O_2^- + 0.2NH_4^+ + 39.62H^+ \rightarrow CH_{1.8}O_{0.5}N_{0.2} + 20.98Fe^{2+} + 5.3HCO_3^- + 52.86H_2O \quad (32)$$

The corresponding Gibbs energy of metabolism, ΔG_{met}, is -417.10 kJ (C-mol biomass)$^{-1}$ and is calculated using Eq. (21).

Eq. (32) is written to yield one C-mol biomass; alternatively, the metabolic formula reaction can be expressed per mol of acetate consumed:

$$6.67Fe(OH)_3 + C_2H_3O_2^- + 0.064NH_4^+ + 12.59H^+ \rightarrow 0.318CH_{1.8}O_{0.5}N_{0.2} + 6.67Fe^{2+} + 1.68HCO_3^- + 16.79H_2O \quad (33)$$

With $\Delta G_{met} = -132.5$ kJ (mol acetate)$^{-1}$. The lower Gibbs energy yield of reaction (33) compared to that of the catabolic reaction (31), -132.5 versus -173.1 kJ (mol acetate)$^{-1}$, reflects that only a fraction of the acetate consumed is used to generate catabolic energy, while the other fraction is allocated to biomass growth. In contrast to catabolism, where acetate is oxidized, during anabolism the carbon in acetate is reduced in order to form new biomass. Consequently, it is important to account for all the carbon utilization, as captured by the metabolic reaction, rather than assume that all of the C-based ED is oxidized.

9. A THERMODYNAMIC LIMIT FOR Y

Minimum catabolic energy requirements to sustain a variety of microbial metabolisms range from -4 to -50 kJ (mol ED)$^{-1}$ (see review by Hoehler (2004)). The lowest catabolic energy yield in our database is -12.7 kJ (mol acetate)$^{-1}$ for acetotrophic methanogenesis by *Methanosarcina mazei*. Thus, below a catabolic Gibbs energy yield (i.e., $-\Delta G_{cat}$) of about 10 kJ (mol ED)$^{-1}$ predicting Y values with GEDYM may no longer be meaningful and, therefore, not recommended by the authors.

There are instances, however, where the catabolic reaction is favourable (i.e., $\Delta G_{cat}<0$), but the corresponding ΔG_{met} is equal or greater than zero (Liu et al., 2007). A zero ΔG_{met} value represents the thermodynamic limit of Y, as one would expect the specific growth rate (μ) to become infinitely slow and the microorganisms would be outgrown by competitors (von Stockar et al., 2006). This intuitively contradictory interplay between Y and μ is a so-called rate-yield trade-off (RYTO) (see Lipson, 2015; and references therein). When ΔG_{met} becomes positive, the metabolic reaction should no longer be able to proceed. Possibly, microorganisms cope with this condition by activating energy overflow or spilling processes (Russell and Cook, 1995).

From a bioenergetics perspective, the growth yield Y reaches its absolute maximum value (Y_{max}) when $\Delta G_{met} = 0$. Substituting the latter condition into Eq. (23) then gives:

$$Y_{max} = \frac{\Delta G_{cat}}{\Delta G_{cat} v - \Delta G_{an}} \quad (34)$$

When applying GEDYM, it is crucial to recognize the existence of an upper limit to Y (i.e., Y_{max}) in order to avoid overestimating growth yields. In the examples described in Section 9, we therefore systematically compare the values of Y and Y_{max} under variable geochemical conditions.

10. GEOCHEMICAL APPLICATIONS OF GEDYM

In many environments, energy supply exerts a key control on geomicrobial activity. In soils, sediments and aquifers, the energy flow sustaining the microbial community usually originates from detrital organic electron donors, with electrons ultimately transferred to internal or external terminal electron acceptors (Thullner et al., 2007; Hoehler and Jorgensen, 2013, and references therein). Fermentation products, for example acetate and H_2, often serve as the direct energy substrates for heterotrophic respiration in the subsurface. As reviewed by Zhuang et al. (2011), in situ acetate oxidation rates range from values as high as 6.4 μM h^{-1} in lake sediments (Lovley and Klug, 1983) to as low as 0.0135 μM h^{-1} in deep aquifers (Chapelle and Lovley, 1990). These rates are well below those measured in the laboratory, even in experiments intended to mimic microbial physiology and slow growth in low energy environments. For example, in acetate-limited flow-through bioreactors designed to derive kinetic parameters (including Y) for *Geobacter sulfurreducens* in groundwater environments, Lin et al. (2009) and Esteve-Nunez et al. (2005) used acetate as the limiting reagent which was supplied at rates of 20 and 220 μM h^{-1}, respectively.

Thus, laboratory-derived Y values may offer poor analogs for growth yields in the subsurface. The distinctive advantage of GEDYM is that it allows for the dynamic adjustment of ΔG_{met}, and therefore Y, when geochemical conditions change. The use of GEDYM is illustrated using the examples of dissimilatory iron reduction, sulfate reduction and methanogenesis, that is, microbial processes that play major roles in the biogeochemical cycling of carbon, nutrients and contaminants in anoxic environments.

10.1. Iron reduction

We expand the iron reduction example of Section 7 by calculating Y values for the dissimilatory reduction of goethite (α-FeOOH) and ferrihydrite ($Fe(OH)_3$) for variable activities of aqueous Fe^{2+} and acetate, at 12 °C and under chemical conditions typical of those encountered in groundwater (Tables C.2 and C.3, Fig. 5, C4-C7). The activities of Fe^{2+} at which the groundwater is in equilibrium with either vivianite ($Fe_3(PO_4)_2$), siderite ($FeCO_3$), magnetite (Fe_3O_4), or mackinawite (FeS), that is, secondary iron minerals commonly forming during Fe(III) reduction, are shown in Fig. 5 (Hansel et al., 2003).

As expected, predicted Y values for reduction of $Fe(OH)_3$ and α-FeOOH increase with increasing acetate activity and decrease with increasing aqueous Fe^{2+} activity (Fig. 5). Furthermore, Y is systematically higher for $Fe(OH)_3$ than α-FeOOH, because of the greater catabolic energy production generated by the reduction of $Fe(OH)_3$. At activities of acetate and Fe^{2+} of 10^{-3} and 10^{-9}, respectively, Y equals 0.261 C-mol biomass (C-mol acetate)$^{-1}$ for $Fe(OH)_3$ and 0.192 C-mol biomass (C-mol acetate)$^{-1}$ for α-FeOOH. At Fe^{2+} activities above $10^{-4.5}$, α-FeOOH reduction becomes thermodynamically unfavourable, with ΔG_{cat} becoming positive (Fig. C4). However, these Fe^{2+} activities are likely rarely reached in the

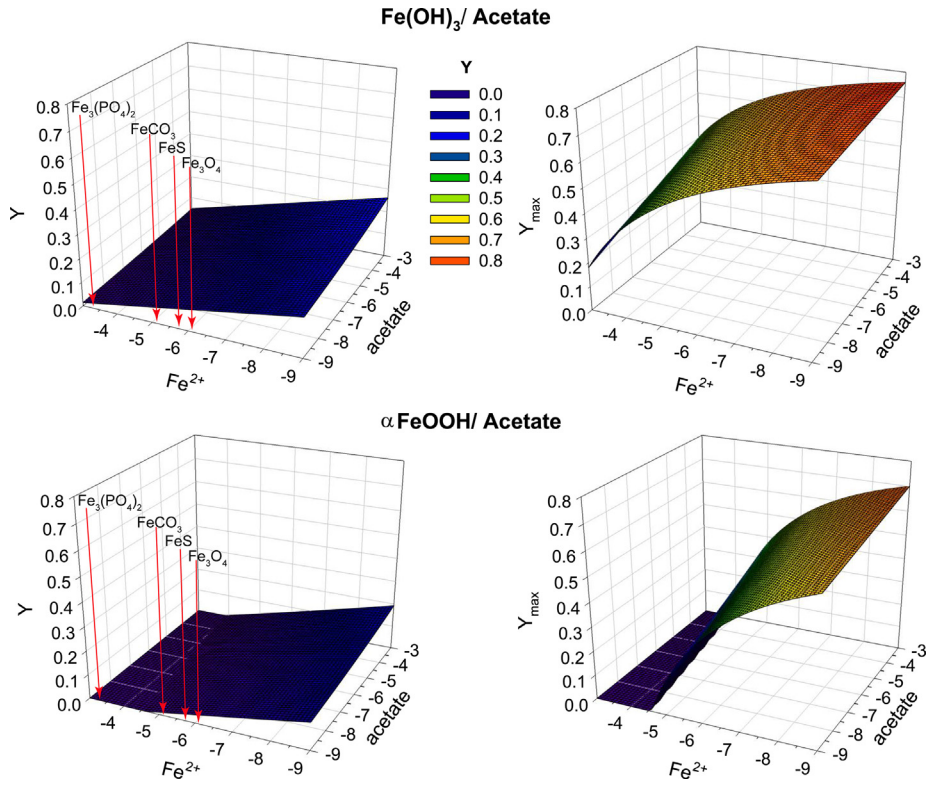

Fig. 5. Predicted Y and Y_{max} as a function of the log acetate and Fe(II) activities for acetate oxidation coupled to Fe(III) reduction in ferrihydrite ($Fe(OH)_3$) and goethite (α-FeOOH). Y and Y_{max} are expressed as C-mol biomass/C-mol acetate. Arrows denote Fe(II) activities when groundwater is in equilibrium with vivianite ($Fe_3(PO_4)_2$), siderite ($FeCO_3$), mackinawite (FeS), and magnetite (Fe_3O_4) as predicted by PHREEQC. Y and Y_{max} values are assigned a value of 0 when Y and Y_{max} values are equal to or less than 0, and ΔG_{cat} is greater than 0.

subsurface as they exceed the solubilities of potential secondary ferrous iron minerals commonly found in reducing environments.

As can also be seen on Fig. 5, the Y_{max} values calculated with Eq. (34) are significantly greater than the corresponding Y values. For the acetate and Fe^{2+} activity ranges covered in Fig. 5, the maximum Y/Y_{max} ratios are 0.34 and 0.27 for $Fe(OH)_3$ and α-FeOOH, respectively (Fig. C7). The marked differences between Y and Y_{max} reflect the large negative values of ΔG_{met}, from −400 to −1200 kJ (C-mol biomass)$^{-1}$ under the geochemical conditions considered (Fig. C5), that is, values that deviate significantly from the $\Delta G_{met} = 0$ condition that defines Y_{max} (Eq. (26)).

The highest Y value for α-FeOOH in Fig. 5, i.e. 0.192 C-mol biomass (C-mol acetate)$^{-1}$, falls at the lower end of growth yields typically assigned to microbial iron reduction in geochemical models, which range from as low as 0.12 (Istok et al., 2010) to 0.40 (Li et al., 2009; Scheibe et al., 2009; Bao et al., 2014) to as high as 0.60 C-mol biomass (C-mol acetate)$^{-1}$ (Watson et al., 2003). Interestingly, despite the higher catabolic energy gained during Fe $(OH)_3$ reduction, lower Y values have been used in geochemical models to represent dissimilatory ferrihydrite reduction, including 0.015 C-mol biomass (C-mol DOC)$^{-1}$ (Eljamal et al., 2011) and 0.03 C-mol biomass (C-mol DOC)$^{-1}$ (Perera et al., 2010), where DOC stands for dissolved organic carbon. Possibly, this results from the lower energy content of naturally occurring DOC compared to acetate.

10.2. Sulfate reduction

Next, we compare Y values for sulfate reduction coupled to the oxidation of H_2 or acetate (Tables C.2 and C.3, Fig. 6, C4-C7). Molecular hydrogen, H_2, is often an important fermentation product in reducing subsurface environments and serves as an electron donor to many microbial metabolisms, including sulfate reduction, dissimilatory Fe (III) reduction and methanogenesis (Caccavo et al., 1992; Lovley et al., 1994; Lovley and Chapelle, 1995). In the calculations, the aqueous sulfide activity is kept constant by assuming equilibrium with mackinawite (FeS), typically the first iron sulfide to form as a result of microbial sulfate reduction (Omoregie et al., 2013). The corresponding activities of HS^- and H_2S at pH 7 are $10^{-6.13}$ and $10^{-6.17}$, respectively. The activities of sulfate, acetate and H_2 are varied from 10^{-9} to 10^{-3}. For H_2, this range is representative of concentrations typically measured in the shallow (e.g, Lovley et al., 1994; Jakobsen and Postma, 1999) and deep terrestrial subsurface (e.g., Li et al., 2016; Hernsdorf et al., 2017).

The calculated Y values fall in the ranges 0.004–0.192 and 0.007–0.079 C-mol biomass (mol acetate or H_2)$^{-1}$, respectively (Fig. 6). The Y values for acetate oxidation

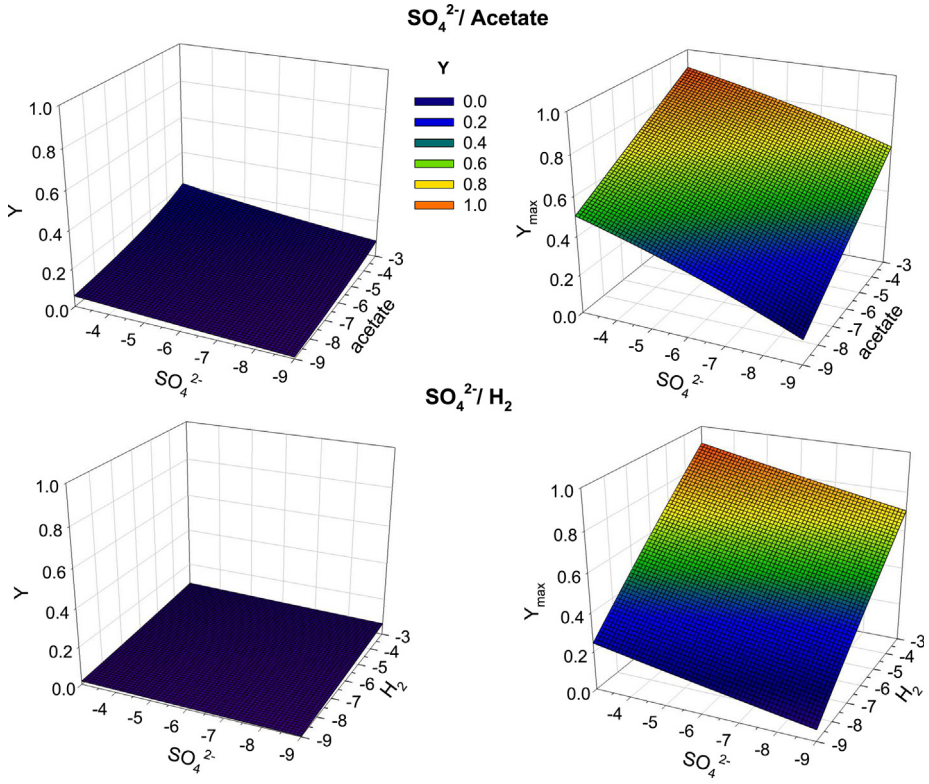

Fig. 6. Predicted Y and Y_{max} for sulfate reduction as a function of log acetate or H_2 and sulfate activities. To compare across metabolisms, Y and Y_{max} are expressed as C-mol biomass/mol acetate or mol H_2.

coupled to sulfate reduction expressed in units of C-mol biomass (C-mol acetate)$^{-1}$ are lower than when $Fe(OH)_3$ and α-FeOOH are the electron acceptors, due to the smaller catabolic energy gains for sulfate reduction (Fig. C4). As for Fe(III) reduction, the calculated Y values are much smaller than the corresponding Y_{max} values for sulfate reduction with acetate and H_2, giving maximum Y/Y_{max} ratios of 0.22 and 0.09, respectively (Fig. C7). This is consistent with the predicted ΔG_{met} values for both sulfate reduction pathways, which stay well below zero, from −260 to −805 kJ (C-mol biomass)$^{-1}$ under the conditions considered (Fig. C5).

Values of Y used to represent sulfate reduction coupled to acetate oxidation in geochemical models span from 0.032 to 0.100 C-mol biomass (C-mol acetate)$^{-1}$ (Watson et al., 2003; Li et al., 2009; Scheibe et al., 2009; Istok et al., 2010; Bao et al., 2014; Cheng et al., 2016). These values fall within our predicted range. Nonetheless, they are implemented as constant parameters and therefore do not reflect changes in ΔG_{cat} and ΔG_{an} whose values may vary considerably depending on the chemical conditions (Figs. C4 and C6). Fewer subsurface geochemical models include sulfate reduction coupled to H_2 oxidation. Istok et al. (2010) assigned a Y value of 0.07 C-mol biomass (mol H_2)$^{-1}$, which is near the high end of the Y range computed for the geochemical conditions examined here (Fig. 6). Based on the results presented in Fig. 6, we would expect Y values to be quite small at the low H_2 concentrations observed in the shallow subsurface (i.e., <10 nM) (Lovley et al., 1994), but higher as H_2 concentrations increase up to the mM concentrations observed in some deeper subsurface environments (Li et al., 2016).

10.3. Methanogenesis

Lastly, we compare Y values for acetotrophic and hydrogenotrophic methanogenesis (Fig. 7). For acetotrophic methanogenesis (AM), the methane and acetate activities are varied, while the HCO_3^- activity is kept constant at $10^{-2.43}$ to reflect equilibrium with calcite (Tables C.2 and C.3). The predicted Y values for hydrogenotrophic methanogenesis (HM) are consistently low, reaching only 0.03 C-mol biomass (mol H_2)$^{-1}$ at the highest H_2 activity considered (10^{-3}). It is important to note that the highest Y value does not coincide with the largest catabolic energy yield ($-\Delta G_{cat} = 40.5$ kJ (mol H_2)$^{-1}$, Fig. C4), which is reached for H_2 and CH_4 activities of 10^{-3} and 10^{-9}, respectively. The explanation resides in the fact that Y not only depends on ΔG_{cat} but also on the values of ΔG_{an} and ΔG_{an}° (Eq. (28), Fig. C6). For autotrophic HM, ΔG_{an}° is actually highly negative, −93.4 kJ (C-mol biomass)$^{-1}$, therefore, as ΔG_{cat} becomes more negative, the denominator in Eq. (28) becomes larger thereby lowering predicted Y values.

The ΔG_{met} values for HM, under the chemical conditions covered in Fig. 7, range from −1800 to +82 kJ (C-mol biomass)$^{-1}$ with the majority of the values more negative than −800 kJ (C-mol biomass)$^{-1}$, which reflects the high

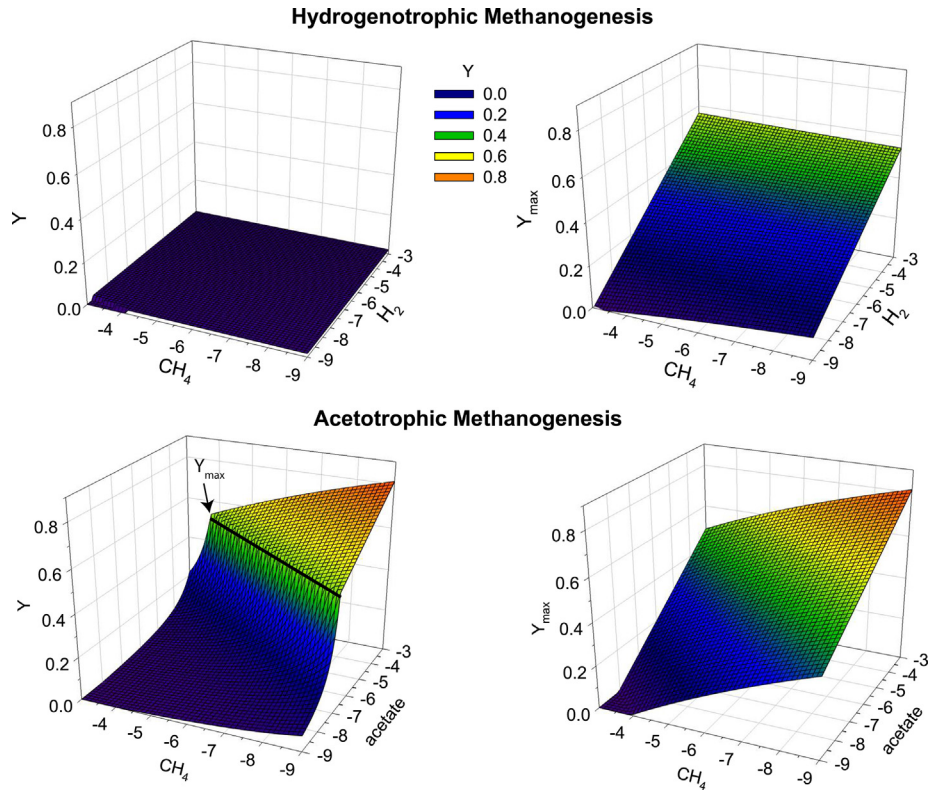

Fig. 7. Predicted Y and Y_{max} for hydrogenotrophic (HM) and acetotrophic methanogenesis (AM) as a function of log acetate or H_2 and methane activities. To compare across metabolisms, Y and Y_{max} are expressed as C-mol biomass/ mol acetate or mol H_2. The black line on the panel representing predicted Y for AM denotes the methane and acetate activities at which Y and Y_{max} converge. Y and Y_{max} values are assigned a value of 0 when Y and Y_{max} values are equal to or less than 0, and ΔG_{cat} is greater than 0.

energetic cost of using HCO_3^- as a carbon source in the anabolic reaction (Fig. C5). Moreover, predicted Y values exceed Y_{max} at high methane activities (10^{-3}) and low H_2 activities (10^{-9}) where ΔG_{met} becomes positive (Figs. C5 and C7). This trend is the result of decreased catabolic energy gains coupled to more positive ΔG_{an} values (Figs. C4 and C6) leading to lower Y_{max} values (Eq. (34)) and, therefore, increasing Y/Y_{max}. When the calculated Y value exceeds Y_{max}, we assign the Y_{max} value predicted using Eq. (34) to Y.

Acetototrophic methanogenesis shows a wider range of predicted Y values than the previous metabolisms, ranging from 0 to 0.8 C-mol biomass (mol acetate)$^{-1}$ (Fig. 7). These results highlight the importance of accounting for variable catabolic and anabolic Gibbs energies calculated under non-standard state conditions. Moreover, at high acetate activities, which correspond to more negative ΔG_{cat} values (Fig. C4), predicted Y values exceed Y_{max} (Figs. 7, C7). Consequently, all of these Y values are assigned the Y_{max} value obtained using Eq. (34). Similar to HM, AM also shows a wide range of ΔG_{met} values from -1696 to $+522$ kJ (C-mol biomass)$^{-1}$, however, in contrast to HM, the majority of ΔG_{met} values for AM are less negative than -800 kJ (C-mol biomass)$^{-1}$ (Fig. C5).

Values of Y for HM used in subsurface biogeochemical models range from 0.015 to 0.020 C-mol biomass (mol H_2)$^{-1}$ (Istok et al., 2010; Tang et al., 2016), that is, values that fall within our predicted Y values. Moreover, in some studies growth via HM is assumed negligible, that is $Y \approx 0$ (e.g., Watson et al., 2003). Values of Y used for AM tend to be higher than for HM, ranging from 0.02 to 0.5 C-mol biomass (mol acetate)$^{-1}$ (Istok et al., 2010; Tang et al., 2016). These higher values are consistent with those obtained here using GEDYM, which range up to 0.8 C-mol biomass (mol acetate)$^{-1}$. The wide range of Y values predicted for AM, coupled to the potential for Y values for both HM and AM to approach or exceed Y_{max}, illustrates the importance of systematically calculating Y_{max} in parallel with Y, in order to avoid predicting growth yields that violate the Second Law of thermodynamics. The latter may happen when relying only on ΔG_{cat}, rather than the full energy mass balance (Section 4), when deciding whether a given metabolism can support growth or not (e.g., Hoehler and Jorgensen, 2013; Blodau, 2011, Blodau et al., 2011).

11. CONCLUSIONS AND FUTURE DIRECTIONS

Geomicrobial activity in environmental systems is closely linked to the generation and allocation of energy by the resident microorganisms. A key parameter in microbial kinetics is the growth yield, Y, which depends on the relative energetics of the catabolic and anabolic reactions. The reaction energetics, in turn, are functions of the geochemical composition and temperature of the medium

surrounding the microbial cells. Existing bioenergetics models, however, do not, or only incompletely, account for variable geochemical conditions. The proposed Gibbs Energy Dynamic Yield Method (GEDYM) overcomes this limitation.

GEDYM is developed and validated using a carefully compiled database of measured growth yields, media compositions, and the associated catabolic and anabolic reaction formulas. For each Y value, the data allow us to derive the overall metabolic reaction formula, and to calculate the Gibbs energies of catabolism (ΔG_{cat}), anabolism (ΔG_{an}) and metabolism (ΔG_{met}). The database further yields a very strong linear relationship between the ratio of the Gibbs energy of metabolism to its standard state value (i.e., $\Delta G_{met}/\Delta G^{\circ}_{met}$) and the corresponding ratio of the Gibbs energy of catabolism (i.e., $\Delta G_{cat}/\Delta G^{\circ}_{cat}$). With this empirical relationship it becomes possible, for any given metabolism, to simultaneously calculate Y, predict the overall metabolic reaction stoichiometry, and calculate the value of ΔG_{met}, as a function of temperature and the activities of reactants and products.

Because GEDYM explicitly represents the effects of changes in geochemical conditions, it provides a new theoretical foundation to iteratively compute Y values and adjust metabolic reaction formulas in biogeochemical reaction models. As shown by the geochemical applications of GEDYM presented here, while the catabolic energy yield (i.e., $-\Delta G_{cat}$) plays a central role in controlling microbial growth yields, depending on the particular metabolism and geochemical environment, the energetics of biomass synthesis (i.e., ΔG_{an}) and the existence of a maximum allowable growth yield (i.e., Y_{max}) also regulate the values of Y.

While GEDYM accounts for the role of the energetics of catabolism and anabolism on microbial growth yields, biomass-explicit models have the flexibility to incorporate other controls on geomicrobial growth kinetics. These models can, for example, explicitly represent the effects of nutrient limitation and species competition, as well as additional energy sinks, for example, energy requirements for maintenance, detoxification, surplus storage or the energy costs associated with the assimilation of nitrogen and sulfur.

ACKNOWLEDGEMENTS

This research was supported by the Canada Excellence Research Chair (CERC) program, the U.S. Department of Energy Subsurface Biogeochemical Research program (Grant No. DE-SC0005520), and the Global Water Futures (GWF) funded under the Canada First Excellence Research Fund (CFREF). We would like to thank Kassandra Ma for her assistance with compiling the growth yield database and the Ecohydrology Research Group for the many thoughtful discussions and insights.

APPENDIX A. SUPPLEMENTARY MATERIAL

Supplementary data associated with this article can be found, in the online version, at https://doi.org/10.1016/j.gca.2018.08.023.

REFERENCES

Andersen K. B. and von Meyenburg K. (1980) Are growth rates of *Escherichia coli* in batch cultures limited by respiration? *J. Bacteriol.* **144**, 114–123.

Arora B., Spycher N. F., Steefel C. I., Molins S., Bill M., Conrad M. E., Dong W., Faybishenko B., Tokunaga T. K., Wan J., Williams K. H. and Yabusaki S. B. (2016) Influence of hydrological, biogeochemical and temperature transients on subsurface carbon fluxes in a flood plain environment. *Biogeochemistry* **127**, 367–396.

Badziong W., Thauer R. K. and Zeikus J. G. (1978) Isolation and characterization of *Desulfovibrio* growing on hydrogen plus sulfate as the sole energy source. *Arch. Microbiol.* **116**, 41–49.

Bao C., Wu H., Li L., Newcomer D., Long P. E. and Williams K. H. (2014) Uranium bioreduction rates across scales: biogeochemical hot moments and hot spots during a biostimulation experiment at Rifle, Colorado. *Environ. Sci. Technol.* **48**, 10116–10127.

Basan M., Hui S., Okano H., Zhang Z., Shen Y., Williamson J. R. and Hwa T. (2015) Overflow metabolism in *Escherichia coli* results from efficient proteome allocation. *Nature* **528**, 99–104.

Battley E. H. (1992) On the calculation of the free energy change accompanying the growth of escherichia coli K-12 on succinic acid. *Biotech. Bioeng.* **39**, 589–595.

Belli K. M., DiChristina T. J., Van Cappellen P. and Taillefert M. (2015) Effects of aqueous uranyl speciation on the kinetics of microbial uranium reduction. *Geochim. Cosmochim. Acta* **157**, 109–124.

Blodau C. (2011) Thermodynamic control on terminal electron transfer and methanogenesis, Aquatic Redox Chemistry. *ACS Publications*, 65–83.

Blodau C., Siems M. and Beer J. (2011) Experimental burial inhibits methanogenesis and anaerobic decomposition in water-saturated peats. *Environ. Sci. Technol.* **45**, 9984–9989.

Caccavo F., Blakemore R. P. and Lovley D. R. (1992) A hydrogen-oxidizing, Fe (III)-reducing microorganism from the Great Bay Estuary, New Hampshire. *Appl. Environ. Microbiol.* **58**, 3211–3216.

Caccavo F., Lonergan D. J., Lovley D. R., Davis M., Stolz J. F. and McInerney M. J. (1994) *Geobacter sulfurreducens* sp. nov., a hydrogen-and acetate-oxidizing dissimilatory metal-reducing microorganism. *Appl. Environ. Microbiol.* **60**, 3752–3759.

Chapelle F. H. and Lovley D. R. (1990) Rates of microbial metabolism in deep coastal plain aquifers. *Appl. Environ. Microbiol.* **56**, 1865–1874.

Cheng Y., Hubbard C. G., Li L., Bouskill N., Molins S., Zheng L., Sonnenthal E., Conrad M. E., Engelbrektson A. and Coates J. D. (2016) Reactive transport model of sulfur cycling as impacted by perchlorate and nitrate treatments. *Environ. Sci. Technol.* **50**, 7010–7018.

Dale A. W., Regnier P. and Van Cappellen P. (2006) Bioenergetic controls on anaerobic oxidation of methane (AOM) in coastal marine sediments: A theoretical analysis. *Am. J. Sci.* **306**, 246–294.

Dong W. and Brooks S. C. (2006) Determination of the formation constants of ternary complexes of uranyl and carbonate with alkaline earth metals (Mg^{2+}, Ca^{2+}, Sr^{2+}, and Ba^{2+}) using anion exchange method. *Environ. Sci. Technol.* **40**, 4689–4695.

Eljamal O., Perera E. and Jinno K. (2011) Practice of mass transport model application for biogeochemical redox process in aquifer. *ISRN Ecol.* **2011**, 1–15.

Esteve-Nunez A., Rothermich M., Sharma M. and Lovley D. (2005) Growth of *Geobacter sulfurreducens* under nutrient-

limiting conditions in continuous culture. *Environ. Microbiol.* **7**, 641–648.

Guillaumont R., Fanghanel V., Neck V., Fuger J., Palmer D. A., Grenthe I. and Rand M. H. (2003) *Update on the Chemical Thermodynamics of Uranium, Neptunium, Plutonium, Americium and Technetium*. Nuclear Energy Agency, Paris, France.

Hansel C. M., Benner S. G., Neiss J., Dohnalkova A., Kukkadapu R. K. and Fendorf S. (2003) Secondary mineralization pathways induced by dissimilatory iron reduction of ferrihydrite under advective flow. *Geochim. Cosmochim. Acta* **67**, 2977–2992.

Heijnen J. and Van Dijken J. (1992) In search of a thermodynamic description of biomass yields for the chemotrophic growth of microorganisms. *Biotechnol. Bioeng.* **39**, 833–858.

Heijnen J., van Loosdrecht M. C. and Tijhuis L. (1992) A black box mathematical model to calculate auto-and heterotrophic biomass yields based on Gibbs energy dissipation. *Biotechnol. Bioeng.* **40**, 1139–1154.

Hernsdorf A. W., Amano Y., Miyakawa K., Ise K., Suzuki Y., Anantharaman K., Probst A., Burstein D., Thomas B. C. and Banfield J. F. (2017) Potential for microbial H_2 and metal transformations associated with novel bacteria and archaea in deep terrestrial subsurface sediments. *ISME J.* **11**, 1915–1929.

Hoehler T. M. (2004) Biological energy requirements as quantitative boundary conditions for life in the subsurface. *Geobiology* **2**, 205–215.

Hoehler T. M. and Jorgensen B. B. (2013) Microbial life under extreme energy limitation. *Nat. Rev. Microbiol.* **11**, 83–94.

Hunter K. S., Wang Y. and Van Cappellen P. (1998) Kinetic modeling of microbially-driven redox chemistry of subsurface environments: coupling transport, microbial metabolism and geochemistry. *J. Hydrol.* **209**, 53–80.

Istok J. D., Park M., Michalsen M., Spain A. M., Krumholz L. R., Liu C., McKinley J., Long P., Roden E., Peacock A. D. and Baldwin B. (2010) A thermodynamically-based model for predicting microbial growth and community composition coupled to system geochemistry: Application to uranium bioreduction. *J. Contam. Hydrol.* **112**, 1–14.

Jakobsen R. and Postma D. (1999) Redox zoning, rates of sulfate reduction and interactions with Fe-reduction and methanogenesis in a shallow sandy aquifer, Rømø, Denmark. *Geochim. Cosmochim. Acta* **63**, 137–151.

Jin Q. and Bethke C. M. (2003) A new rate law describing microbial respiration. *Appl. Environ. Microbiol.* **69**, 2340–2348.

Jin Q. and Bethke C. M. (2007) The thermodynamics and kinetics of microbial metabolism. *Am. J. Sci.* **307**, 643–677.

Jin Q., Roden E. E. and Giska J. R. (2013) Geomicrobial kinetics: extrapolating laboratory studies to natural environments. *Geomicrobiol. J.* **30**, 173–185.

Kleerebezem R. and Van Loosdrecht M. C. M. (2010) A generalized method for thermodynamic state analysis of environmental systems. *Crit. Rev. Environ. Sci. Technol.* **40**, 1–54.

Laanbroek H. J., Geerligs H. J., Sijtsma L. and Veldkamp H. (1984) Competition for sulfate and ethanol among *Desulfobacter*, *Desulfobulbus*, and *Desulfovibrio* species isolated from intertidal sediments. *Appl. Environ. Microbiol.* **47**, 329–334.

LaRowe D. E. and Amend J. P. (2015) Catabolic rates, population sizes and doubling/replacement times of microorganisms in natural settings. *Am. J. Sci.* **315**, 167–203.

LaRowe D. E., Dale A. W., Amend J. P. and Van Cappellen P. (2012) Thermodynamic limitations on microbially catalyzed reaction rates. *Geochim. Cosmochim. Acta* **90**, 96–109.

Li L., Steefel C. I., Williams K. H., Wilkins M. J. and Hubbard S. S. (2009) Mineral transformation and biomass accumulation associated with uranium bioremediation at Rifle, Colorado. *Environ. Sci. Technol.* **43**, 5429–5435.

Li L., Wing B., Bui T., McDermott J., Slater G., Wei S., Lacrampe-Couloume G. and Lollar B. S. (2016) Sulfur mass-independent fractionation in subsurface fracture waters indicates a long-standing sulfur cycle in Precambrian rocks. *Nat. Commun.* **7**, 1–9.

Lin B., Westerhoff H. V. and Roling W. F. (2009) How Geobacteraceae may dominate subsurface biodegradation: physiology of Geobacter metallireducens in slow-growth habitat-simulating retentostats. *Environ. Microbiol.* **11**, 2425–2433.

Lipson D. A. (2015) The complex relationship between microbial growth rate and yield and its implications for ecosystem processes. *Front. Microbiol.* **6**, 1–5.

Liu C., Zachara J. M., Gorby Y. A., Szecsody J. E. and Brown C. F. (2001a) Microbial reduction of Fe (III) and sorption/precipitation of Fe(II) on *Shewanella putrefaciens* strain CN32. *Environ. Sci. Technol.* **35**, 1385–1393.

Liu J. S., Marison I. and Von Stockar U. (2001b) Microbial growth by a net heat up-take: a calorimetric and thermodynamic study on acetotrophic methanogenesis by *Methanosarcina barkeri*. *Biotechnol. Bioeng.* **75**, 170–180.

Liu J. S., Vojinović V., Patiño R., Maskow T. and von Stockar U. (2007) A comparison of various Gibbs energy dissipation correlations for predicting microbial growth yields. *Thermochim. Acta* **458**, 38–46.

Lovley D. R. and Chapelle F. H. (1995) Deep subsurface microbial processes. *Rev. Geophys.* **33**, 365–381.

Lovley D. R., Chapelle F. H. and Woodward J. C. (1994) Use of dissolved H_2 concentrations to determine distribution of microbially catalyzed redox reactions in anoxic groundwater. *Environ. Sci. Technol.* **28**, 1205–1210.

Lovley D. R. and Klug M. J. (1983) Sulfate reducers can outcompete methanogens at freshwater sulfate concentrations. *Appl. Environ. Microbiol.* **45**, 187–192.

Mahadevan R., Palsson B. O. and Lovley D. R. (2011) In situ to in silico and back: elucidating the physiology and ecology of *Geobacter* spp. using genome-scale modelling. *Nat. Rev. Microbiol.* **9**, 39–50.

Majzlan J., Navrotsky A. and Schwertmann U. (2004) Thermodynamics of iron oxides: Part III. Enthalpies of formation and stability of ferrihydrite ($\sim Fe(OH)_3$), schwertmannite ($\sim FeO(OH)_{3/4}(SO_4)_{1/8}$), and ε-Fe_2O_3. *Geochim. Cosmochim. Acta* **68**, 1049–1059.

McCarty P. L. (2007) Thermodynamic electron equivalents model for bacterial yield prediction: modifications and comparative evaluations. *Biotechnol. Bioeng.* **97**, 377–388.

Methe B., Nelson K. E., Eisen J., Paulsen I. T., Nelson W., Heidelberg J., Wu D., Wu M., Ward N. and Beanan M. (2003) Genome of *Geobacter sulfurreducens*: metal reduction in subsurface environments. *Science* **302**, 1967–1969.

Monod J. (1949) The growth of bacterial cultures. *Annu. Rev. Microbiol.* **3**, 371–394.

Neill C. and Gignoux J. (2006) Soil organic matter decomposition driven by microbial growth: A simple model for a complex network of interactions. *Soil. Biol. Biochem.* **38**, 803–811.

Omoregie E. O., Couture R.-M., Van Cappellen P., Corkhill C. L., Charnock J. M., Polya D. A., Vaughan D., Vanbroekhoven K. and Lloyd J. R. (2013) Arsenic bioremediation by biogenic iron oxides and sulfides. *Appl. Environ. Microbiol.* **79**, 4325–4335.

Parkhurst D. L. and Appelo C. (2013) *Description of input and examples for PHREEQC version 3: a computer program for speciation, batch-reaction, one-dimensional transport, and inverse geochemical calculations*. Geological Survey, US.

Perera E. D. P., Jinno K. and Hiroshiro Y. (2010) Bacteria-mediated Reduction and Precipitation of $Fe(OH)_3$ and FeS in the Subsurface of a Coastal Aquifer: A Numerical Investigation. *Water Qual. Expo. Health* **2**, 15–30.

Pirt S. (1965) The maintenance energy of bacteria in growing cultures. *Proc. Royal Soc. Lond.* **163**, 224–231.

Reed D. C., Algar C. K., Huber J. A. and Dick G. J. (2014) Gene-centric approach to integrating environmental genomics and biogeochemical models. *Proc. Natl. Acad. Sci. U.S.A.* **111**, 1879–1884.

Roden E. E. and Jin Q. S. (2011) Thermodynamics of microbial growth coupled to metabolism of glucose, ethanol, short-chain organic acids, and hydrogen. *Appl. Environ. Microbiol.* **77**, 1907–1909.

Rodríguez-Escales P., Folch A., Vidal-Gavilan G. and van Breukelen B. M. (2016) Modeling biogeochemical processes and isotope fractionation of enhanced in situ biodenitrification in a fractured aquifer. *Chem. Geol.* **425**, 52–64.

Roels J. A. (1980) Application of macroscopic principles to microbial metabolism. *Biotechnol. Bioeng.* **22**, 2457–2514.

Russell J. B. and Cook G. M. (1995) Energetics of bacterial growth: balance of anabolic and catabolic reactions. *Microbiol. Rev.* **59**, 48–62.

Rutgers M., van der Gulden H. M. and Dam K. (1989) Thermodynamic efficiency of bacterial growth calculated from growth yield of *Pseudomonas oxalaticus* OX1 in the chemostat. *Biochim. Biophys. Acta, Bioenergy* **973**, 302–307.

Scheibe T. D., Fang Y., Murray C. J., Roden E. E., Chen J., Chien Y.-J., Brooks S. C. and Hubbard S. S. (2006) Transport and biogeochemical reaction of metals in a physically and chemically heterogeneous aquifer. *Geosphere* **2**, 220.

Scheibe T. D., Mahadevan R., Fang Y., Garg S., Long P. E. and Lovley D. R. (2009) Coupling a genome-scale metabolic model with a reactive transport model to describe in situ uranium bioremediation. *Microb. Biotechnol.* **2**, 274–286.

Shock E. L. (1995) Organic acids in hydrothermal solutions: standard molal thermodynamic properties of carboxylic acids and estimates of dissociation constants at high temperatures and pressures. *Am. J. Sci.* **295**, 496–580.

Shock E. L., Sassani D. C., Willis M. and Sverjensky D. A. (1997) Inorganic species in geologic fluids: correlations among standard molal thermodynamic properties of aqueous ions and hydroxide complexes. *Geochim. Cosmochim. Acta* **61**, 907–950.

Smith M. R. and Mah R. A. (1978) Growth and methanogenesis by *Methanosarcina strain* 227 on acetate and methanol. *Appl. Environ. Microbiol.* **36**, 870–879.

Strohm T. O., Griffin B., Zumft W. G. and Schink B. (2007) Growth yields in bacterial denitrification and nitrate ammonification. *Appl. Environ. Microbiol.* **73**, 1420–1424.

Stumm W. and Morgan J. J. (1996) *Aquatic Chemistry: Chemical Equilibria and Rates in Natural Waters*. Wiley, New York.

Tang G., Zheng J., Xu X., Yang Z., Graham D. E., Gu B., Painter S. L. and Thornton P. E. (2016) Biogeochemical modeling of CO_2 and CH_4 production in anoxic Arctic soil microcosms. *Biogeosciences* **13**, 5021–5041.

Thullner M., Regnier P. and Van Cappellen P. (2007) Modeling microbially induced carbon degradation in redox-stratified subsurface environments: concepts and open questions. *Geomicrobiol. J.* **24**, 139–155.

van Breukelen B. M., Griffioen J., Roling W. F. and van Verseveld H. W. (2004) Reactive transport modelling of biogeochemical processes and carbon isotope geochemistry inside a landfill leachate plume. *J. Contam. Hydrol.* **70**, 249–269.

VanBriesen J. M. (2002) Evaluation of methods to predict bacterial yields using thermodynamics. *Biodegradation* **13**, 171–190.

von Stockar U., Maskow T., Liu J., Marison I. W. and Patino R. (2006) Thermodynamics of microbial growth and metabolism: an analysis of the current situation. *J. Biotechnol.* **121**, 517–533.

Wang Z., Liu C., Wang X., Marshall M. J., Zachara J. M., Rosso K. M., Dupuis M., Fredrickson J. K., Heald S. and Shi L. (2008) Kinetics of reduction of Fe(III) complexes by outer membrane cytochromes MtrC and OmcA of *Shewanella oneidensis* MR-1. *Appl. Environ. Microbiol.* **74**, 6746–6755.

Watson I. A., Oswald S. E., Mayer K. U., Wu Y. and Banwart S. A. (2003) Modeling kinetic processes controlling hydrogen and acetate concentrations in an aquifer-derived microcosm. *Environ. Sci. Technol.* **37**, 3910–3919.

Yabusaki S. B., Fang Y., Long P. E., Resch C. T., Peacock A. D., Komlos J., Jaffe P. R., Morrison S. J., Dayvault R. D., White D. C. and Anderson R. T. (2007) Uranium removal from groundwater via in situ biostimulation: Field-scale modeling of transport and biological processes. *J. Contam. Hydrol.* **93**, 216–235.

Zhao J., Scheibe T. D. and Mahadevan R. (2011) Model-based analysis of the role of biological, hydrological and geochemical factors affecting uranium bioremediation. *Biotechnol. Bioeng.* **108**, 1537–1548.

Zhuang K., Izallalen M., Mouser P., Richter H., Risso C., Mahadevan R. and Lovley D. R. (2011) Genome-scale dynamic modeling of the competition between *Rhodoferax* and *Geobacter* in anoxic subsurface environments. *ISME J.* **5**, 305–316.

Associate editor: Ann Pearson